Suppression of Unwanted *ZZ* Interactions in a Hybrid Two-Qubit System

Jaseung Ku,[1] Xuexin Xu,[2,3] Markus Brink,[4] David C. McKay,[4] Jared B. Hertzberg,[4] Mohammad H. Ansari,[2,3] and B. L. T. Plourde[1,*]

[1]*Department of Physics, Syracuse University, Syracuse, New York 13244, USA*
[2]*Peter Grünberg Institute, Forschungszentrum Jülich, Jülich 52428, Germany*
[3]*Jülich-Aachen Research Alliance (JARA), Fundamentals of Future Information Technologies, Jülich 52428, Germany*
[4]*IBM Quantum, IBM T.J. Watson Research Center, Yorktown Heights, New York 10598, USA*

(Received 8 April 2020; accepted 2 September 2020; published 11 November 2020)

Mitigating crosstalk errors, whether classical or quantum mechanical, is critically important for achieving high-fidelity entangling gates in multiqubit circuits. For weakly anharmonic superconducting qubits, unwanted *ZZ* interactions can be suppressed by combining qubits with opposite anharmonicity. We present experimental measurements and theoretical modeling of two-qubit gate error for gates based on the cross resonance interaction between a capacitively shunted flux qubit and a transmon, and demonstrate the elimination of the *ZZ* interaction.

DOI: 10.1103/PhysRevLett.125.200504

Building a fault-tolerant quantum computer requires not only highly coherent qubits but also tailored interactions between qubits for implementing high-fidelity two-qubit entangling gates. Superconducting qubits are a promising candidate [1–4], however, the gate errors in current devices are not definitively below the threshold required for fault tolerance. Despite tremendous improvements in qubit coherence, circuit design, and control, two-qubit gate errors remain in the range of $4\text{–}9 \times 10^{-3}$ [5,6]. This is worse than what would be naively expected based on current device coherences [7]. One limiting factor to these errors is crosstalk in the device corresponding to unwanted terms in the Hamiltonian. This is a particular concern for one of the more common superconducting qubit architectures, fixed-frequency transmons [8] coupled to nearest neighbors via a static exchange term J. In this architecture, the two-qubit gate is enabled by activating the cross-resonance (CR) effect [9–11], where a ZX interaction term is generated by driving one qubit (the control) at the frequency of the neighboring qubit (the target).

The strength of the CR effect is proportional to J [12], and this J also produces an always-on ZZ coupling term. The static ZZ coupling originates from level repulsion between the energy level with both qubits in the first excited state and some noncomputational energy levels and is a consequence of two competing qubit-qubit interactions. Such a ZZ interaction, whether static or driven during the CR gate [12], is an ever-present source of error. Unlike classical crosstalk, which can be canceled by the application of compensation tones [6,12], the ZZ term leads to unwanted entanglement between pairs and so is not easily mitigated unless, for example, additional circuitry, such as a tunable coupler, is added [13,14].

For a transmon-transmon system, which has a negative value of the anharmonicity—the difference between the primary transition out of the qubit subspace and the qubit transition itself—there is no symmetry in the competing interactions and so ZZ is always nonzero. As an alternative approach, if the transmon can be combined with a qubit design where the anharmonicity is positive, the symmetry in the two competing interactions can cause the ZZ term to be canceled at specific qubit-qubit detunings. In this way, the CR effect between two opposite-anharmonicity qubits can be utilized to form a high-fidelity gate. Fortunately, such a qubit exists—the capacitively shunted flux qubit (CSFQ) [15]. Recently, the CSFQ has regained attention, in part, due to its greatly improved coherence time [16]. Although the CSFQ is a flux-tunable device, it can be operated at a flux sweet spot (flux bias $f = \Phi/\Phi_0 = 0.5$, where $\Phi_0 = h/2e$, h is Planck's constant, and e is the electron charge), where it is first-order insensitive to flux noise. The anharmonicity at the sweet spot can be positive and large ($> +500$ MHz), which provides a parameter regime that is otherwise inaccessible in all-transmon devices.

In this Letter we present measurements of the first such hybrid CSFQ-transmon device and theoretical modeling to investigate its performance. First, we experimentally demonstrate and theoretically model the suppression of the static ZZ interaction for a particular detuning of the CSFQ and transmon. Second, we investigate the characteristic behavior of the CR effect as a function of CSFQ-transmon detuning. Third, we explore the dependence of two-qubit gate error on both flux and gate length. Finally, we use our model to describe the requirements for a future device capable of achieving a two-qubit gate error of 1×10^{-3}.

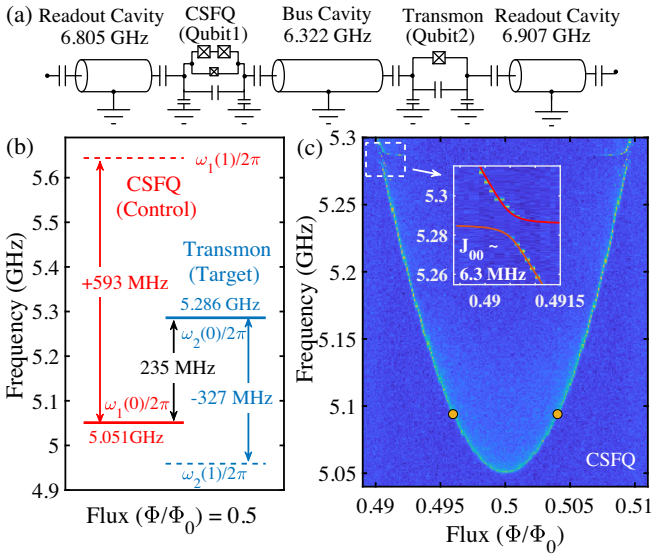

FIG. 1. (a) Simplified circuit diagram of CSFQ-transmon system coupled via a bus cavity. (b) Frequency diagram of transmon and CSFQ at flux sweet spot. (c) CSFQ qubit frequency spectrum vs external magnetic flux. Orange dots indicate flux points where static ZZ becomes zero. (Inset) Anticrossing of transmon and CSFQ with fit (red solid line).

The device consists of a fixed-frequency transmon and CSFQ coupled via a bus cavity resonator [Fig. 1(a)]. Each qubit has its own readout cavity with a microwave port for input and output. Details on sample fabrication, measurement setup, and device parameters can be found in the Supplemental Material [17]. This coupled two-qubit system can be described by the Hamiltonian

$$H = \sum_{q=1,2}\sum_{n_q} \omega_q(n_q)|n_q+1\rangle\langle n_q+1| + \sqrt{(n_1+1)(n_2+1)} \times J_{n_1,n_2}(|n_1+1,n_2\rangle\langle n_1,n_2+1| + \text{H.c.}), \quad (1)$$

where $\omega_q(n_q)$ is the bare transition frequency between energy levels n_q and n_q+1 for qubit q. The primary qubit transition is thus $\omega_q(0)$ and we define $\omega_q \equiv \omega_q(0)$. The coupling strength J_{n_1,n_2} provides an indirect two-photon interaction via a bus cavity between energy levels n_1 and n_1+1 in qubit 1 and levels n_2 and n_2+1 in qubit 2 (see Supplemental Material [17] for details). We take $\hbar = 1$ throughout.

The qubits were measured using conventional circuit-QED techniques in the dispersive regime [35]. At the sweet spot, the measured primary qubit frequency and anharmonicity are (5.051 GHz, +593 MHz) for the CSFQ, and (5.286 GHz, −327 MHz) for the transmon, and thus the qubit-qubit detuning is 235 MHz [Fig. 1(b)]. The bus cavity and readout cavity frequencies for the CSFQ and transmon are (6.322, 6.805, 6.907) GHz, respectively [Fig. 1(a)]. The tunability of the CSFQ spectrum as a function of flux [Fig. 1(c)] allows us to explore a range of qubit-qubit detuning in the following experiments. We fit the anticrossing between the CSFQ and transmon [Fig. 1(c) inset] to obtain the zeroth-order exchange coupling strength $J_{00}/2\pi = 6.3$ MHz. The average single-qubit gate fidelity was measured with the standard randomized benchmarking (RB) protocol (details in the Supplemental Material [17]), giving the average gate error lower than 1×10^{-3}. For CR operation, the fastest CR rates occur when the 0-1 transition frequency for the target qubit falls between the 0-1 and 1-2 transition frequencies of the control qubit [12]. For our system, we achieve this condition by choosing the CSFQ as the control qubit with its 0-1 frequency below that of the transmon, which is the target qubit. With such an arrangement, the much larger anharmonicity of the CSFQ results in a larger frequency window for fast CR rates, which can help to alleviate frequency crowding issues in systems with many qubits.

We investigate how the static ZZ interaction of the system varies with the flux bias of the CSFQ. The effective Hamiltonian that is diagonal in the dressed frame is

$$H_{\text{eff}} = -\tilde{\omega}_1\frac{ZI}{2} - \tilde{\omega}_2\frac{IZ}{2} + \zeta\frac{ZZ}{4}, \quad (2)$$

where $\tilde{\omega}_1$ and $\tilde{\omega}_2$ are the dressed qubit frequencies. ζ is the frequency shift of one qubit when the other qubit is excited from the ground state: $\zeta = (E_{11} - E_{10}) - (E_{01} - E_{00})$, where E_{ij} is the energy eigenvalue of the Hamiltonian for qubit 1 at $|i\rangle$ and qubit 2 at $|j\rangle$. The static ZZ interaction arises when higher energy levels are involved in the two-qubit Hamiltonian. ZZ interaction results in an additional phase rotation depending on the state of either qubit, thus contributing to the two-qubit gate error. ZZ-free qubit pairs can be obtained if ζ vanishes in Eq. (2). A detailed analysis involving block diagonalization of the multilevel Hamiltonian [Eq. (1)] into the qubit subspace shows that ζ can be expressed as (see Supplemental Material [17])

$$\zeta = -\frac{2J_{01}^2}{\Delta+\delta_2} + \frac{2J_{10}^2}{\Delta-\delta_1}, \quad (3)$$

where $\Delta = \omega_2 - \omega_1$ is the qubit-qubit detuning, and $\delta_i = \omega_i(1) - \omega_i$ is the anharmonicity of qubit i. Within the limit $|\Delta| < |\delta|$, where the CR effect is strongest [37], for a transmon-transmon device, both terms of Eq. (3) are positive, and thus ZZ interactions will always be present in all-transmon circuits with fixed couplings. However, in a CSFQ-transmon circuit the second term in Eq. (3) can be negative, due to the large and positive anharmonicity of the CSFQ. Note that for a hybrid CSFQ-transmon device, J_{01} is not necessarily equal to J_{10}, in contrast to a transmon-transmon system where they are almost the same. This allows the hybrid CSFQ-transmon system to be static ZZ-free. For our device, the static ZZ strength has a

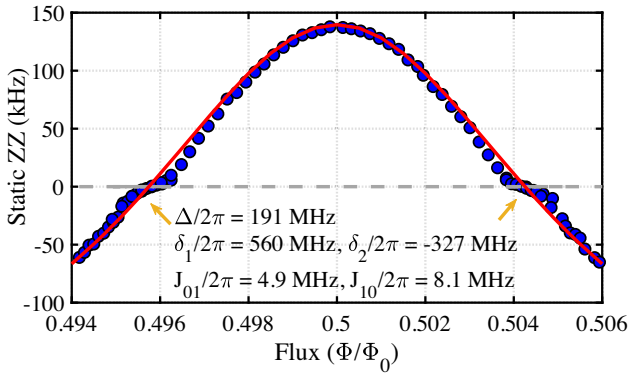

FIG. 2. Static ZZ measured as a function of flux via joint amplification of ZZ (JAZZ) protocol [36]. Error bars are comparable with or smaller than the size of the data symbols. Red solid line represents a theory calculation using Eq. (3). Static ZZ becomes zero at two flux points (0.496, 0.504), and the corresponding device parameters are shown in the plot.

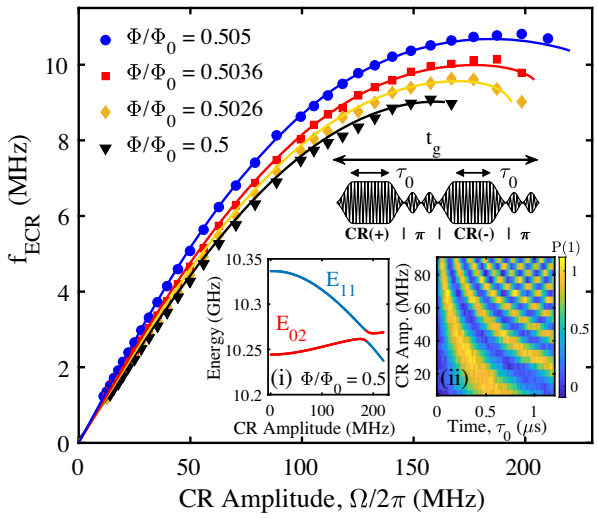

FIG. 3. Echoed CR rate vs CR amplitude at four representative flux points. The corresponding qubit-qubit detunings are (234, 217, 199, 166) in MHz. Solid lines correspond to theoretical model. Inset (i): Computed energy levels of E_{11} and E_{02} vs CR amplitude. Inset (ii): Color density plot of the oscillation of target qubit driven with various CR amplitudes at sweet spot with CSFQ (control) in ground state. Color bar represents first excited state probability of target qubit. Echoed CR pulse sequence illustrated above inset plots.

maximum value of 140 kHz at the flux sweet spot, but away from this point it decreases and eventually crosses zero near $\Phi/\Phi_0 = 0.496$ and 0.504 (Fig. 2). Equation (3) was used to compute the flux dependence of the static ZZ strength using separately extracted device parameters, including the flux-dependent anharmonicity and transition frequencies of the CSFQ (red solid line in Fig. 2). The agreement between theory and experiment is quite good except near the zero-crossing points, where the experimental ZZ data exhibits a kink. We speculate that this could be due to the breakdown of our perturbative treatment of the effective Hamiltonian, and thus Eq. (3). Away from the flux sweet spot, the qubit-qubit detuning decreases, while J_{10} increases, thus pushing the ratio J/Δ beyond the dispersive limit. A framework for treating such situations is discussed in Ref. [38].

Although we have engineered a ZZ suppression in the two-qubit system, it is necessary that we can still perform a fast two-qubit gate using the CR effect. To perform a CR gate, we apply to the control qubit (CSFQ) a tone at the frequency of the target qubit (transmon). This CR drive causes the target qubit state to rotate in a direction that depends on the control qubit state, and thus corresponds to a ZX term in the two-qubit effective Hamiltonian [12]. To suppress undesired ZI and IX terms, we employ an echoed CR pulse (ECR) that consists of two Gaussian flat-top CR pulses with π phase difference, and a π pulse on the control qubit after each CR pulse (Fig. 3 inset) [10]. Thus we define the two-qubit gate length to be $t_g = 2\tau_0 + 160$ ns, where τ_0 is the flat-top length of each CR pulse; the constant 160 ns corresponds to the sum of the rising and falling edges on the CR pulses and the π pulses applied to the control qubit. In Fig. 3, we present the ensuing oscillation frequency f_{ECR} of the transmon as a function of the CR amplitude at different flux bias points. We measure the CR oscillations of the transmon as a function of τ_0 for a range of CR amplitudes [Fig. 3 inset (ii)], where the CR amplitude was calibrated in terms of the Rabi frequency of the CSFQ at the flux sweet spot. In order to extract f_{ECR}, we perform two separate measurements, with the CSFQ in the ground (excited) state initially. Because of the echo sequence and the fact that we measure the z component of the target qubit state vector, the oscillations should be identical in both cases [6], which we confirm by performing both measurements. We then average the two oscillations together and compute f_{ECR}. At low CR amplitude, f_{ECR} increases almost linearly, as expected from first-order perturbation theory. For intermediate drives, f_{ECR} deviates from linearity as the CSFQ is driven off-resonantly [9]. For even larger CR amplitude, f_{ECR} approaches a maximum, which occurs when the energy levels E_{11} and E_{02} are ac-Stark shifted into resonance [Fig. 3 inset (i)]. Applying a nonperturbative diagonalization scheme to the effective Hamiltonian [Eq. (2)] together with a CR driving Hamiltonian, we simulated f_{ECR} vs CR amplitude (details in the Supplemental Material [17]). The resulting theoretical curves for f_{ECR} vs CR amplitude agree well with the experimental points (Fig. 3).

The average two-qubit error per gate was measured via standard RB [39] at various flux points and gate lengths t_g of the ZX_{90}, which serves as the pulse primitive for the two-qubit entangling gate [10] (Fig. 4). For each flux point, the primitive single-qubit gate (X_{90}) and two-qubit gate (ZX_{90}) were recalibrated. No active cancellation pulse for removing classical crosstalk [6] was used. The RB data was fit to the standard fidelity decay curve $A\alpha^m + B$, where m is the

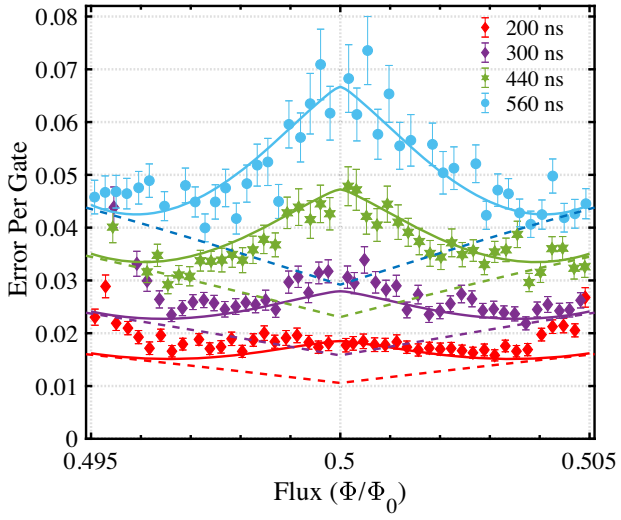

FIG. 4. Average error per two-qubit gate plotted vs flux for four representative gate lengths. Dashed lines indicate theoretical coherence-limited two-qubit gate errors with no ZZ interactions; full theory simulations shown by solid lines.

number of Clifford gates and α the depolarization parameter [39]. The average two-qubit error per gate ϵ was then calculated using the expression, $\epsilon = (3/4)(1-\alpha^{1/N})$, where N is the average number of ZX_{90} gates per two-qubit Clifford gate [40,41].

By increasing the gate length, a characteristic "W"-shaped pattern develops with respect to flux, corresponding to larger errors at the sweet spot with minima to either side, followed by increasing error for further flux biasing away from 0.5. The smallest gate error, 1.6×10^{-2}, occurs for $t_g = 200$ ns and $f = 0.496, 0.504$ (Fig. 4), where the static ZZ becomes zero. This behavior can be described by the interplay between fidelity loss from the ZZ interaction and classical crosstalk on the one hand, and fidelity gain from longer coherence times near the sweet spot on the other hand. Away from the sweet spot, the ZZ interaction and classical crosstalk decrease and the gate fidelity approaches the coherence limit. Including the ZZ interaction and classical crosstalk in our simulation was sufficient to reproduce the flux-dependence of the experimental gate errors.

The coherence-limited gate error (dashed lines in Fig. 4) is mainly dominated by T_2 of the CSFQ, which is 15 μs at the sweet spot but quickly decreases with flux due to flux noise (see plot of T_2 vs flux in the Supplemental Material [17]). This is shorter than T_1, which is 18 μs (40 μs) for the CSFQ (transmon) and T_2 for the transmon, which is 45 μs. As is clear from Fig. 4, the coherence-limit curves alone are not sufficient to reproduce the measured flux-dependence of the gate error. The static ZZ strength (Fig. 2) has a significant impact on the gate error, and was included in the simulation. Moreover, we model classical crosstalk in a similar manner to Ref. [12], by including in the CR driving Hamiltonian a modified amplitude $R(f, t_g)\Omega$ and shifted phase, where $R(f, t_g)$ is a scaling factor. R was modeled using a CR tomography measurement [6] (more details in the Supplemental Material [17]). Ω is the CR amplitude that can be obtained from the experimental ZX_{90} pulse calibrations for each flux and gate length. Simulations agree well with data (Fig. 4). Based on the success of our theoretical model in describing the measured flux- and gate-length dependence of the two-qubit gate error, we consider target parameters for a future device to achieve further reductions in gate error. In Fig. 5, we simulate the two-qubit gate error vs t_g for three sets of coherence times in μs: $(T_1^{(1)}, T_2^{(1)}, T_1^{(2)}, T_2^{(2)})$, where the superscripts indicate the qubit, are (18, 15, 40, 45), (40, 54, 43, 67), and (200, 200, 200, 200), corresponding respectively to the present device, the two-transmon device in Ref. [6], and a hypothetical, but within reach, device. We note that leakage effects out of the 0-1 subspace for each qubit due to the CR drive are negligible for the gate times considered in Fig. 5 since the energy difference between E_{11} and E_{02} [e.g., Fig. 3 inset (i)] is relatively large for CR amplitudes below 100 MHz. From the discussion above, we know that one of the most prominent advantages of a CSFQ-transmon device over a transmon-transmon device is that the static ZZ interaction can be canceled by carefully choosing qubit parameters. To realize such an idealized static ZZ-free device, one could use a weakly tunable asymmetric transmon [42] coupled to a CSFQ held at its sweet spot. Such a

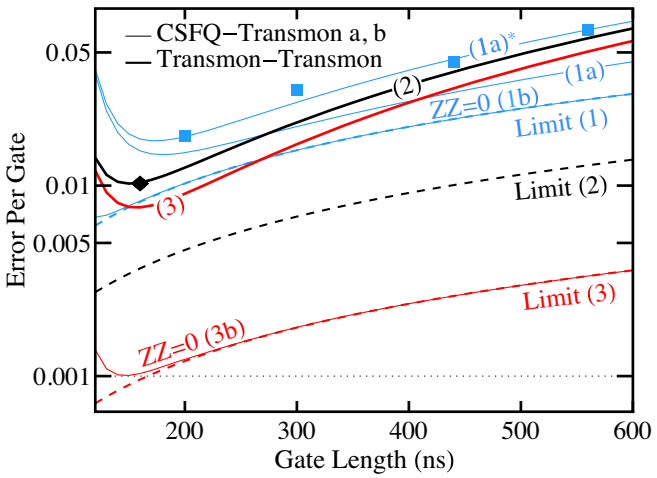

FIG. 5. Experimental data and theory simulation for two-qubit gate error vs gate length for our present CSFQ-transmon (a), static ZZ-free CSFQ-transmon (b), and a transmon-transmon device with nonzero ZZ (thick lines). The CSFQ was placed at sweet spot. Square CR pulses were used in theory simulation. Three sets of coherence times used in simulation were color-coded in blue, black, and red, and numbered by $n = \{1, 2, 3\}$. "Limit (n)" represents the coherence-limited gate error. Classical crosstalk is not included except $(1a)^*$. Blue squares and black diamond are experimental data points from present device and Ref. [6], respectively.

device should achieve coherence times at least as long as our present experimental device, while maximizing T_2 of the CSFQ at the $ZZ = 0$ point, thus enabling a gate error (1b) comparable to the best transmon-transmon results (2). For the projected longer coherence times (200 μs) [43,44], the gate error (3b) of such a device subject to elimination of classical crosstalk can reach 1×10^{-3}. This level is inaccessible for a transmon-transmon device, even with the projected longer coherence times (3). While coherence-limited gate errors (dashed lines in Fig. 5) decrease monotonically with gate length, the total error reaches a minimum at an optimum gate length. This is a universal behavior, even in the absence of static ZZ or classical crosstalk [e.g., (3b) in Fig. 5]. It can be explained by the dynamic ZZ that arises from strong CR drive [45,46]. Since larger CR amplitude is required for shorter gate length and the dynamic ZZ scales quadratically with CR amplitude [45,46], at short gate times a large ZZ interaction can still occur, which thus limits the minimum gate error.

In conclusion, we have characterized the CR gate on a CSFQ-transmon device. This hybrid system with opposite anharmonicity between the qubits allows for the complete suppression of the static ZZ interaction, which becomes essential for achieving a high-fidelity CR gate. Our theoretical analysis shows that suppressing the ZZ interaction is just as important as enhancing coherence times. By eliminating the spurious ZZ interaction, a CSFQ-transmon gate can achieve comparable fidelities to a transmon-transmon gate despite having shorter coherence times. With longer coherence times that are not too far beyond current experimental capabilities (200 μs), two-qubit gate errors of 1×10^{-3} are feasible.

We thank David DiVincenzo, Sarah Sheldon, and Jerry Chow for helpful discussions, and acknowledge support from Intelligence Advanced Research Projects Activity (IARPA) under Contract No. W911NF-16-1-0114. D. M. acknowledges support by the Army Research Office under Contract No. W911NF-14-1-0124.1

Note added—Recenty, we became aware of related theoretical work on ZZ interactions between transmons and CSFQs in Ref. [47].

*Corresponding author.
bplourde@syr.edu

[1] J. Clarke and F. K. Wilhelm, Nature (London) **453**, 1031 (2008).
[2] M. H. Devoret and R. J. Schoelkopf, Science **339**, 1169 (2013).
[3] J. M. Gambetta, J. M. Chow, and M. Steffen, npj Quantum Inf. **3**, 2 (2017).
[4] P. Krantz, M. Kjaergaard, F. Yan, T. P. Orlando, S. Gustavsson, and W. D. Oliver, Appl. Phys. Lett. **6**, 021318 (2019).
[5] F. Arute *et al.*, Nature (London) **574**, 505 (2019).
[6] S. Sheldon, E. Magesan, J. M. Chow, and J. M. Gambetta, Phys. Rev. A **93**, 060302(R) (2016).
[7] K. X. Wei, I. Lauer, S. Srinivasan, N. Sundaresan, D. T. McClure, D. Toyli, D. C. McKay, J. M. Gambetta, and S. Sheldon, Phys. Rev. A **101**, 032343 (2020).
[8] J. Koch, T. M. Yu, J. Gambetta, A. A. Houck, D. I. Schuster, J. Majer, A. Blais, M. H. Devoret, S. M. Girvin, and R. J. Schoelkopf, Phys. Rev. A **76**, 042319 (2007).
[9] J. M. Chow, A. D. Córcoles, J. M. Gambetta, C. Rigetti, B. R. Johnson, J. A. Smolin, J. R. Rozen, G. A. Keefe, M. B. Rothwell, M. B. Ketchen, and M. Steffen, Phys. Rev. Lett. **107**, 080502 (2011).
[10] A. D. Córcoles, J. M. Gambetta, J. M. Chow, J. A. Smolin, M. Ware, J. Strand, B. L. T. Plourde, and M. Steffen, Phys. Rev. A **87**, 030301(R) (2013).
[11] V. Tripathi, M. Khezri, and A. N. Korotkov, Phys. Rev. A **100**, 012301 (2019).
[12] E. Magesan and J. M. Gambetta, Phys. Rev. A **101**, 052308 (2020).
[13] F. Yan, P. Krantz, Y. Sung, M. Kjaergaard, D. L. Campbell, T. P. Orlando, S. Gustavsson, and W. D. Oliver, Phys. Rev. Applied **10**, 054062 (2018).
[14] P. Mundada, G. Zhang, T. Hazard, and A. Houck, Phys. Rev. Applied **12**, 054023 (2019).
[15] M. Steffen, S. Kumar, D. P. DiVincenzo, J. R. Rozen, G. A. Keefe, M. B. Rothwell, and M. B. Ketchen, Phys. Rev. Lett. **105**, 100502 (2010).
[16] F. Yan, S. Gustavsson, A. Kamal, J. Birenbaum, A. P. Sears, D. Hover, T. J. Gudmundsen, D. Rosenberg, G. Samach, S. Weber, J. L. Yoder, T. P. Orlando, J. Clarke, A. J. Kerman, and W. D. Oliver, Nat. Commun. **7**, 12964 (2016).
[17] See Supplemental Material at http://link.aps.org/supplemental/10.1103/PhysRevLett.125.200504 for device parameters, theory details and other miscellaneous information, which includes Refs. [18–34].
[18] A. Potts, G. Parker, J. Baumberg, and P. de Groot, Meas. Technol. **148**, 225 (2001).
[19] A. D. Córcoles, J. M. Chow, J. M. Gambetta, C. Rigetti, J. R. Rozen, G. A. Keefe, M. B. Rothwell, M. B. Ketchen, and M. Steffen, Appl. Phys. Lett. **99**, 181906 (2011).
[20] M. F. Gely, G. A. Steele, and D. Bothner, Phys. Rev. A **98**, 053808 (2018).
[21] S. Sheldon, M. Sandberg, H. Paik, B. Abdo, J. M. Chow, M. Steffen, and J. M. Gambetta, Appl. Phys. Lett. **111**, 222601 (2017).
[22] L. S. Cederbaum, J. Schirmer, and H. D. Meyer, J. Phys. A **22**, 2427 (1989).
[23] D. P. DiVincenzo, *Quantum Information Processing: Lecture Notes of the 44th IFF Spring School 2013* (Forschungszentrum, Jülich, 2013).
[24] J. M. Epstein, A. W. Cross, E. Magesan, and J. M. Gambetta, Phys. Rev. A **89**, 062321 (2014).
[25] F. Yoshihara, K. Harrabi, A. O. Niskanen, Y. Nakamura, and J. S. Tsai, Phys. Rev. Lett. **97**, 167001 (2006).
[26] M. Rol, F. Battistel, F. Malinowski, C. Bultink, B. Tarasinski, R. Vollmer, N. Haider, N. Muthusubramanian, A. Bruno, B. Terhal, and L. DiCarlo, Phys. Rev. Lett. **123**, 120502 (2019).

[27] S. S. Hong, A. T. Papageorge, P. Sivarajah, G. Crossman, N. Didier, A. M. Polloreno, E. A. Sete, S. W. Turkowski, M. P. da Silva, and B. R. Johnson, Phys. Rev. A **101**, 012302 (2020).
[28] J. Braumüller, L. Ding, A. Vepslinen, Y. Sung, M. Kjaergaard, T. Menke, R. Winik, D. Kim, B. M. Niedzielski, A. Melville, J. L. Yoder, C. F. Hirjibehedin, T. P. Orlando, S. Gustavsson, and W. D. Oliver, Phys. Rev. Applied **13**, 054079 (2020).
[29] A. P. Sears, A. Petrenko, G. Catelani, L. Sun, H. Paik, G. Kirchmair, L. Frunzio, L. I. Glazman, S. M. Girvin, and R. J. Schoelkopf, Phys. Rev. B **86**, 180504 (2012).
[30] J. R. Garbow, D. P. Weitekamp, and A. Pines, Chem. Phys. Lett. **93**, 504 (1982).
[31] F. Motzoi, J. M. Gambetta, P. Rebentrost, and F. K. Wilhelm, Phys. Rev. Lett. **103**, 110501 (2009).
[32] S. Kimmel, G. H. Low, and T. J. Yoder, Phys. Rev. A **92**, 062315 (2015).
[33] S. Sheldon, L. S. Bishop, E. Magesan, S. Filipp, J. M. Chow, and J. M. Gambetta, Phys. Rev. A **93**, 012301 (2016).
[34] J. M. Gambetta, A. D. Córcoles, S. T. Merkel, B. R. Johnson, J. A. Smolin, J. M. Chow, C. A. Ryan, C. Rigetti, S. Poletto, T. A. Ohki, M. B. Ketchen, and M. Steffen, Phys. Rev. Lett. **109**, 240504 (2012).
[35] A. Blais, R.-S. Huang, A. Wallraff, S. M. Girvin, and R. J. Schoelkopf, Phys. Rev. A **69**, 062320 (2004).
[36] M. Takita, A. W. Cross, A. D. Corcoles, J. M. Chow, and J. M. Gambetta, Phys. Rev. Lett. **119**, 180501 (2017).
[37] M. Ware, B. R. Johnson, J. M. Gambetta, T. A. Ohki, J. M. Chow, and B. L. T. Plourde, arXiv:1905.11480.
[38] M. H. Ansari, Phys. Rev. B **100**, 024509 (2019).
[39] E. Magesan, J. M. Gambetta, and J. Emerson, Phys. Rev. Lett. **106**, 180504(R) (2011).
[40] D. C. McKay, C. J. Wood, S. Sheldon, J. M. Chow, and J. M. Gambetta, Phys. Rev. A **96**, 022330 (2017).
[41] D. C. McKay, S. Sheldon, J. A. Smolin, J. M. Chow, and J. M. Gambetta, Phys. Rev. Lett. **122**, 200502 (2019).
[42] M. D. Hutchings, J. B. Hertzberg, Y. Liu, N. T. Bronn, G. A. Keefe, M. Brink, J. M. Chow, and B. L. T. Plourde, Phys. Rev. Applied **8**, 044003 (2017).
[43] K. Serniak, S. Diamond, M. Hays, V. Fatemi, S. Shankar, L. Frunzio, R. J. Schoelkopf, and M. H. Devoret, Phys. Rev. Applied **12**, 014052 (2019).
[44] IBM Research Blog, Cramming More Power Into a Quantum Device (2019), https://www.ibm.com/blogs/research/2019/03/power-quantum-device/.
[45] X. Xu and M. H. Ansari, arXiv:2009.00485.
[46] M. Malekakhlagh, E. Magesan, and D. C. McKay, arXiv:2005.00133.
[47] P. Zhao, P. Xu, D. Lan, J. Chu, X. Tan, H. Yu, and Y. Yu, Preceding Letter, Phys. Rev. Lett. **125**, 200503 (2020).